Transport in Porous Media **35:** 189–204, 1999.

Use of Magnetic Resonance Imaging as a Tool for the Study of Foamy Oil Behavior for an Extra-Heavy Crude Oil. T_2/Viscosity Correlation with Respect to Pressure

DOUGLAS B. FISHER[1], JOUSSEF ESPIDEL[2,⋆], MARLENE HUERTA[3], LESLIE RANDALL[1] and JON GOLDMAN[1]
[1]*Petroleum Recovery Institute, Calgary, Canada;* [2]*Departamento de Análisis y Evaluación, INTEVEP, S.A., Apartado Postal 76343, Caracas 1070A, Venezuela;* [3]*Departamento de Yacimientos, INTEVEP, S.A., Apartado Postal 76343, Caracas 1070A, Venezuela*

(Received: 13 August 1998)

Abstract. The purpose of this work is to present the results of the phase behavior study for a live heavy oil during a pressure depletion process using magnetic resonance imaging (MRI) as a tool to characterize foamy oil phenomena. The experiments were carried out in the pressure range of 13.1 to 1.4 MPa. Signal intensity images were obtained at each pressure and with respect to time, that is, approximately for a total time of 3 h after each pressure change. It is possible to see a variation in intensity across the sample. These changes can be associated with changes in mobility as well as segregation of the oil. It was also possible to observe that what we trust is the formation of gas channels at the last two pressure values, as it comes out of solution. A correlation between the transverse relaxation time T_2 and temperature was established with the aim of producing one between T_2 and viscosity. In this way viscosity maps for the live oil were obtained as a function of pressure and time. It was observed that above the bubble point, the viscosity maps varied from low to high to low with respect to time for the same pressure. Below the bubble point the situation is reverse. The viscosity map changes from high to low to high with respect to time for the same pressure. The study shows the potential use of MRI to follow viscosity changes during pressure depletion test in a PVT MRI cell.

Key words: MRI, foamy oil, maps, T_2, viscosity.

1. Introduction

The use of conventional phase behavior measurements in heavy oils has always been a problem, due to the extreme optical density and viscosity found in this type of oil. With the interest in 'foamy oil' and its properties, the need to get some physical phase behavior data becomes more important. In this respect, the presence of dissolved gas in highly viscous oils and the subsequent formation of small gas bubbles during a pressure depletion test is believed to play an important role in improving its flow characteristics.

⋆ Author to whom correspondence should be addressed

Recently, a report has been presented by Fisher *et al.* (1995), which used magnetic resonance imaging (MRI) as an aid to visualize dynamic phase behavior as gas bubbles come out of solution. The idea of using MRI as a tool for the study of these systems lies in the fact that optical density is not a factor in providing an image of the interface between the oil and gas. The NMR signal is based on the number of hydrogen atoms in the oil. The gas has a lower density as well as a lower hydrogen content, and as such will not give a significant NMR signal. MRI allows us to measure NMR properties anywhere within the oil which can then be correlated to some physical characteristic of the gas-crude oil system.

Some of the NMR parameters involved are the variation of the signal intensity of the image as a function of pressure and time, and the Transverse relaxation time T_2, when measured using the Carre–Purcell–Meiboom–Gill (CPMG) pulse sequence. Regarding T_2, there is the possibility of obtaining two different values. On the one hand, there is the so-called 'bulk' relaxation for the sample as a whole. On the other hand, there is the T_2 mapping that gives a value for each pixel of the image from the particular image section. A correlation between T_2 values with viscosity changes in the sample can then be obtained. This could give valuable information about the behavior of the sample as a function of pressure change and time. We are therefore assuming that images generated using MRI will allow us to visualize dynamic phase behavior as bubbles of gas come out of solution in either stable emulsion like assemblages or rise to the top by gravity segregation and bubble nucleation.

The purpose of this paper is to present MRI results obtained from the study of phase behavior characteristic of Hamaca crude oil under a pressure depletion process. Here, we will be presenting results based on the initial work by Fisher *et al.* (1995). These included intensity maps, changes in T_2 with respect to pressure and time, and correlation between T_2 maps and viscosity.

2. Experimental Conditions

A sample of Hamaca crude oil, with a dead oil viscosity of 3300 MPa s at 60°C, was mixed with methane gas at a pressure of 10.3, and a temperature of 60°C. The top schematic in Figure 1(a) shows a diagram of the set up used to saturate the oil. An outline of the recombination procedure is as follows: (i) A sample of oil in the transferred vessel was heated at 60°C; (ii) then, the methane was added to bring the pressure up to 10.3 MPa; (iii) the oil was recirculated, and additional methane was added over a period of several days to keep the working pressure constant; (iv) Step (iii) was repeated until no change in the pressure was observed; (v) The system was left to settle to allow a single-phase oil/gas system to form. Finally, the pressure of the system was increased to 13.1 MPa, the initial pressure for the MRI experiments.

The sample was then transferred to a nonmagnetic core holder, designed at the Petroleum Recovery Institute (PRI) for the pressure and temperature working conditions. Figure 1(b) shows a diagram of the MRI core holder, which will now be referred to as a phase behavior (PVT) cell. The transfer process was done by displacing heated

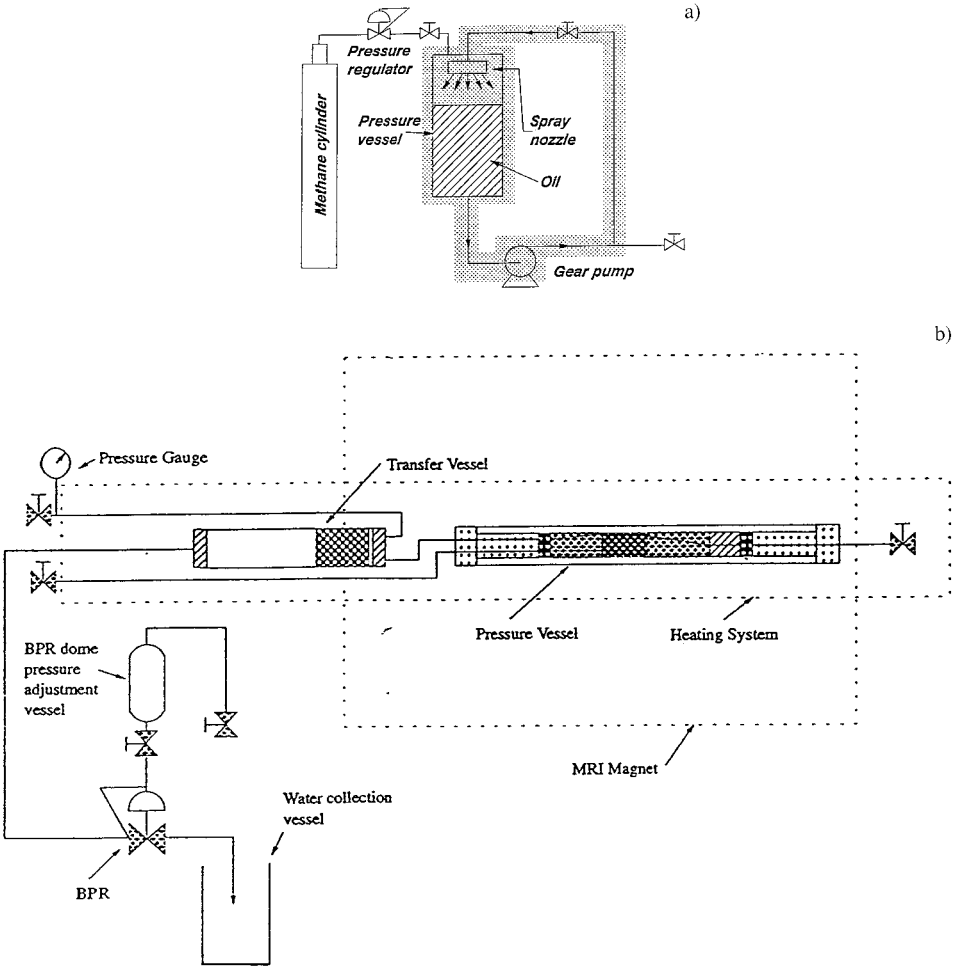

Figure 1. (a) Oil recombination equipment; (b) foamy oil equipment schematic, and MRI PVT cell core holder.

dead oil inside the PVT cell with the recombined Hamaca oil, and it is described as follows: (i) The whole PVT cell and tubing system was kept at a working temperature of 60°C; (ii) dead oil was transferred to the PVT cell, and the pressure was increased up to 13.1 MPa; (iii) the recombined oil was pumped into the PVT cell through the top valve displacing the dead oil through the bottom valve. Approximately three cell volumes, 150 ml, were used to insure that no dead oil was left inside. After the oil was transferred, the PVT cell was laid to rest inside the magnet for 24 h before any MRI experiment was performed. After this period, images were taken before and after the PVT cell was turned by 180°. The purpose of this was to ensure that we had started with a homogeneous one-phase sample.

The basic phase behavior sequence was to keep the temperature and sample mass constant and to reduce the pressure in steps of approximately 1.2 MPa by increasing

the volume of the sample. These pressure changes are considered to be slow pressure drops. The MRI variable temperature system was used to keep the PVT cell at a constant temperature in the magnet. The experiment was conducted at several discrete pressure steps from either 13.1 to 1.4 MPa, at each pressure the rate of change of pressure from the last pressure was as fast as the back pressure regulator (BPR) could be reset. The average time period over which MRI measurements were made was 3 h.

All MRI experiments were carried out on a BRUKER 100 MHz Biospec spectrometer. Image reconstruction was performed with the UXNMR program provided by BRUKER using the X-32 UNIX based computer. Multi-Slice Single-Echo images (MSME-SE), signal profiles and Multi-Slice Multi-Echo (MSME-ME) T_2 relaxation maps measurements were obtained as a function of both time and pressure. Bulk T_2 values were also measured using the Carre–Purcell–Meiboom–Gill pulse sequence (CPMG).

3. Results and Discussion

Individual bubbles are not observed in the MRI experiments partially due to the in-plane resolution (625 μm on a side), which is larger than the expected diameter of the bubbles. This is partially due to the voxel volume (20 mm thick), which means that in a single voxel a large number of bubbles would be averaged, if present. The presence of the gas bubbles will be detected by a decreased voxel intensity since they occupy a given volume of the voxel and consequently less oil will be present (Figure 2). Methane in the gas phase does not give rise to an appreciable NMR signal. From this relationship alone, it would be expected that regions of the sample that have a very significant low signal intensity would be described as locations in the

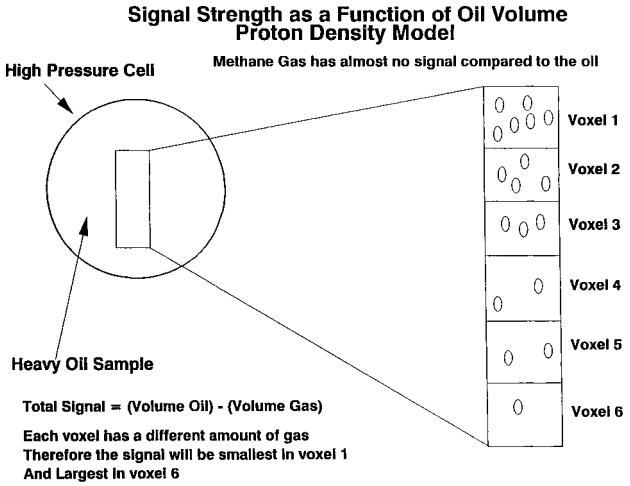

Figure 2. Signal strength as a function of oil volume. Proton density model.

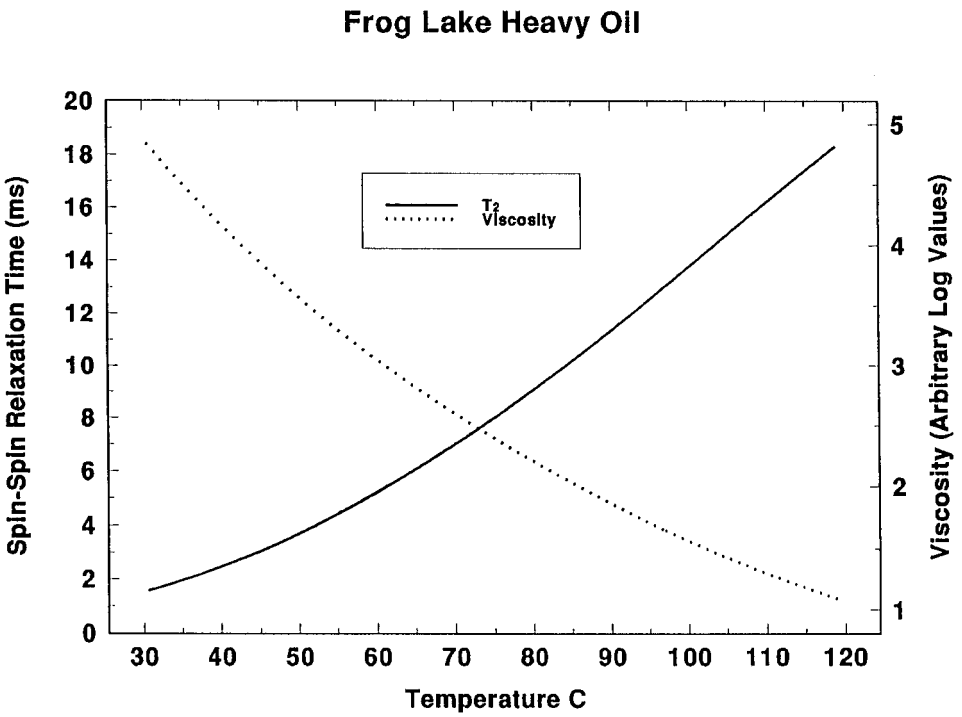

Figure 3. Correlation of Spin–Spin relaxation time and viscosity correlation versus temperature.

PVT cell where gas phase is concentrated. At high pressures, we are working with a single-phase gas/oil system, that is, gas dissolved in the crude. Below the bubble point, there is a phase transition for the gas. Those areas with very low or no signal intensity, which are shown in the images as an upgoing path, will be referred to as regions where gas is coming out of solution as gas bubbles or gas channels.

The signal intensity in an image is, however, affected by another parameter known as the spin–spin relaxation time constant (T_2). As the spin–spin relaxation time constant T_2 increases, the signal intensity increases. This means that regions of the sample which have longer T_2 relaxation time constants will have higher signal intensities. The opposite occurs for short T_2values. The changes in intensity produced by this effect will be more gradual than those produced by a high gas bubbles concentration.

Morris *et al.* (1994) found that there is an inverse relationship between the spin–spin relaxation constant and kinematic viscosity for bulk oils ranging from 1 to 100 000 MPa s. As the viscosity decreases, the T_2 constant increases. This inverse relationship between T_2 and viscosity has also been observed at the PRI for a heavy oil from Frog Lake, Alberta. It is well-known that for heavy oils the viscosity decreases as the temperature increases. From Figure 3, it can be seen that as the temperature increases, the viscosity decreases and T_2 increases. The relationship between T_2, viscosity and signal intensity means that, at a constant temperature, regions of the

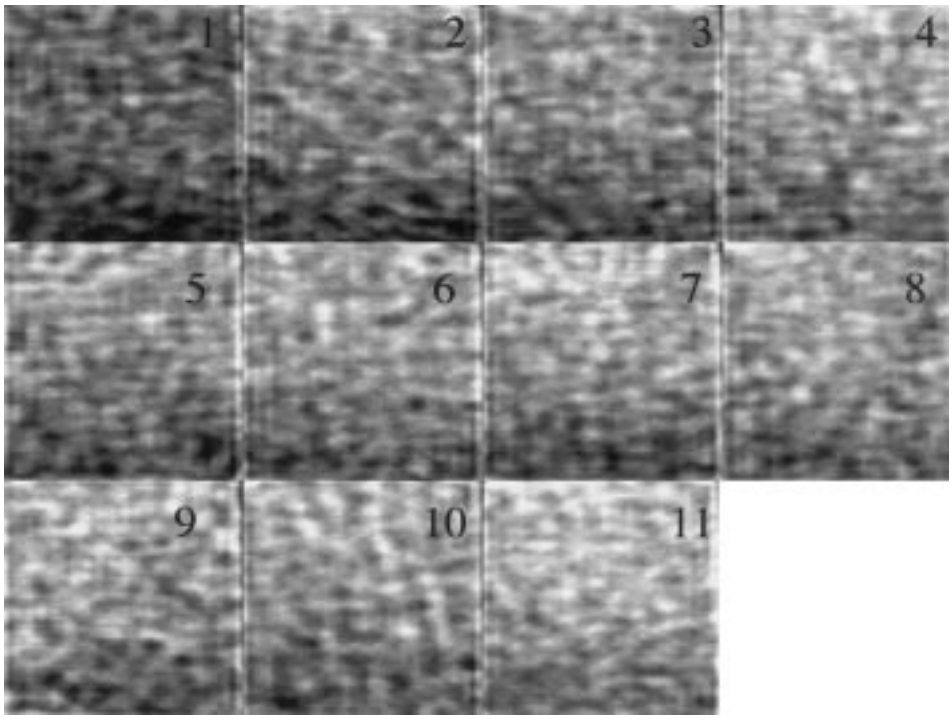

Figure 4. Image signal variation with respect to time after the pressure change: pressure 11.2 MPa. Time between images is of the order of 15 min. The number position in the image indicates the top of the PVT cell.

sample which have different viscosities will have different signal intensities. The lower the viscosity, the higher the signal intensity.

The overall distribution of gas bubbles in the PVT cell can be detected from an analysis of the voxel intensity patterns (Fisher, 1995). If the distribution of gas bubbles is uniform across the whole sample or if no gas bubbles are present, then no detectable variations in the signal strength across the image in any direction should be observed. If the viscosity of the oil changes across the sample or if gas is present in sufficient quantity to reduce the oil volume, then signal intensity variations should occur.

3.1. SIGNAL INTENSITY BEHAVIOR WITH RESPECT TO PRESSURE AND TIME

Single echo images were taken from the Hamaca live oil at each pressure, and various times after the pressure change. These images are presented in Figures 4–7 for 11.2, 7.6, 3.4 and 1.4 MPa; the highest pressure being above the reported bubble point for this crude. All detectable changes observed in these images after the pressure steps are attributed to effects produced by these processes as the sample reaches equilibrium.

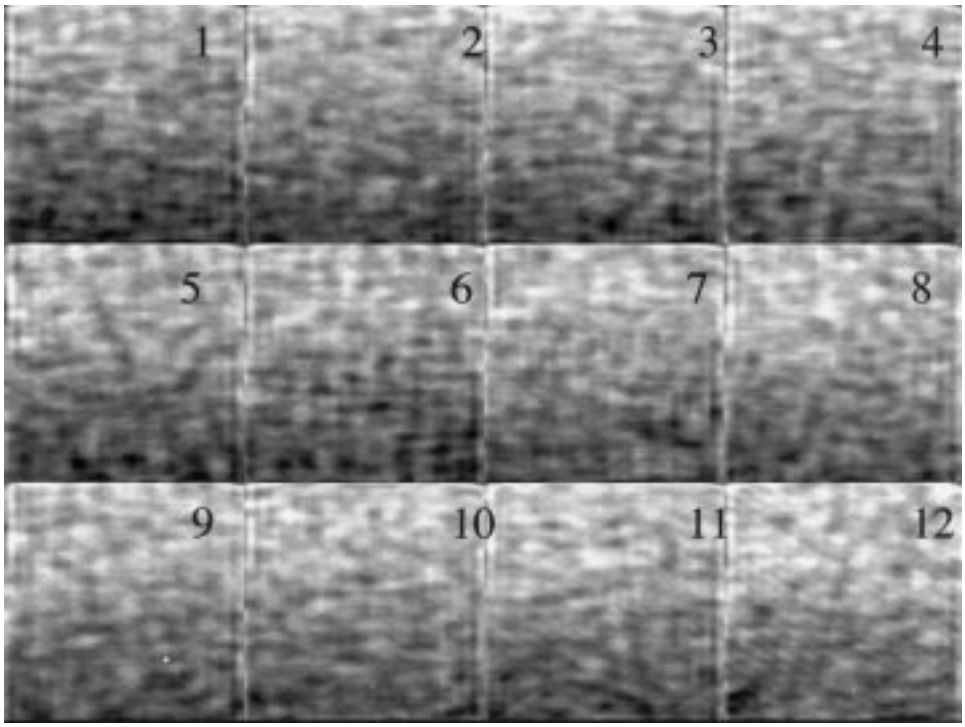

Figure 5. Image signal variation with respect to time after the pressure change: pressure 7.6 MPa. Time between images is of the order of 15 min. The number position in the image indicates the top of the PVT cell.

In Figure 4 (11.2 MPa), it is possible to see a progressive increase of signal intensity for the sample with respect to time. This variation can be translated into an increased mobility of the nuclear spins within the sample, produced by the pressure change, in the process to reach the equilibrium state. This increased mobility would be a consequence of the changes in viscosity experienced by the system as time increases after the pressure change. These changes in viscosity might be related to the rearrangement of the dissolved gas within the sample. It is also possible to see small segregation from the top to the bottom of the sample. For this particular pressure and with respect to time, the formation of gas channels was not observed as it is expected at pressures above the bubble point. The same phenomena described above is observed at 7.6 MPa (Figure 5). But at this point the segregation between high and low intensity is bigger. In other words, the area of low intensity is increasing at the expense of the area of high intensity.

For the present work, the gas channel formation was not detected until the pressure was as low as 3.4 MPa (Figure 6). The presence of a gas cap was just detectable about 2 h after the pressure change, and well formed after 4 h. From this result and compared to earlier work done by Fisher *et al.* (1995), it can be concluded that the detectable liberation of gas to form channels is a kinetic controlled process that depends on the

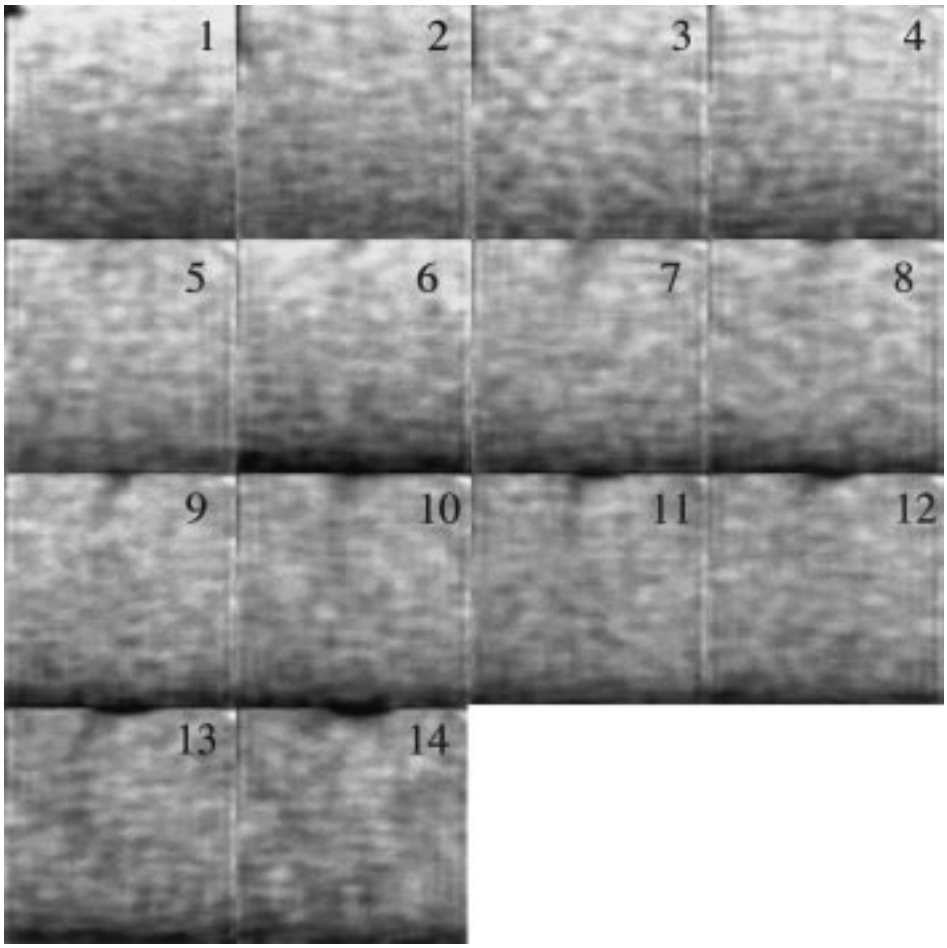

Figure 6. Image signal variation with respect to time after the pressure change: pressure 3.4 MPa. Time between images is of the order of 15 min. The number position in the image indicates the top of the PVT cell.

size of pressure drop used in the experiment. This is in agreement with earlier results presented by Maini (1995).

At the lowest pressure (1.4 MPa, Figure 7), the changes in signal intensity and the formation of gas channels are more dramatic. After the pressure change, there is a uniform distribution of intensities along the sample. In less than half an hour, there is a drastic reduction in intensity, and at the same time it is possible to observe the presence of gas channels. There is a continuous increase of the gas cap within an hour, and then it remains constant. The gas channels are less and less evident up to a point where they can no longer be detected.

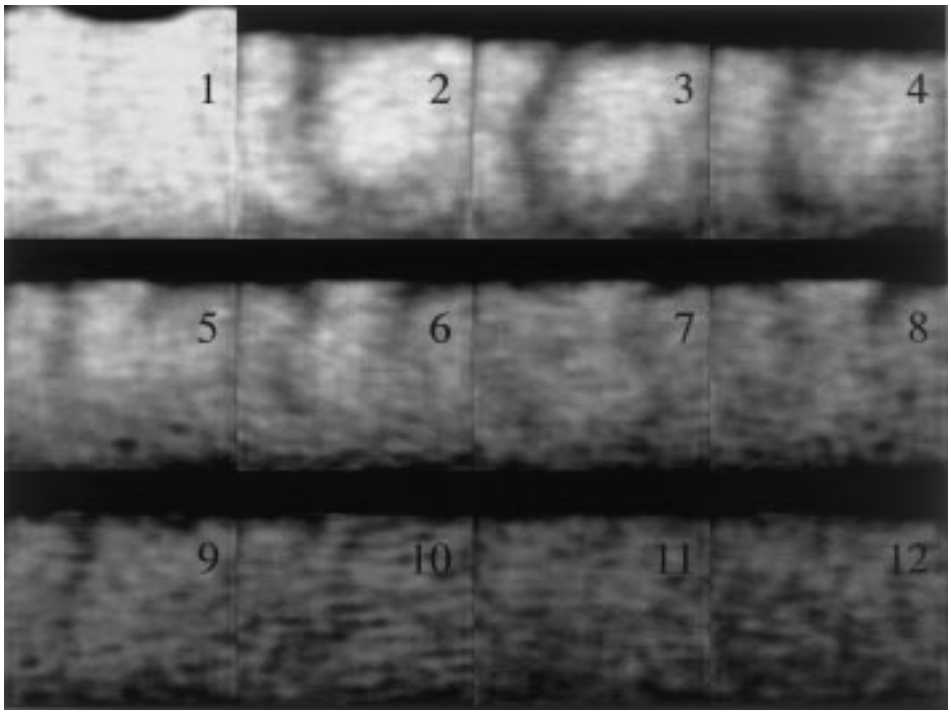

Figure 7. Image signal variation with respect to time after the pressure change: pressure 1.4 MPa. Time between images is of the order of 15 min. The number position in the image indicates the top of the PVT cell.

3.2. TRANSVERSE, T_2, RELAXATION MAPS BEHAVIOR WITH RESPECT TO PRESSURE AND TIME

One of the purposes of this work was to measure the transverse relaxation time, T_2, for every pixel of image by means of the Multi-Slice Multi-Echo experiment (MSME-ME). In this way, T_2 maps for a whole section of the sample can be obtained. It is important to note that due to the way the experiment is performed, it is only possible to detect the long T_2 components present in the sample.

An example of such a map is presented in Figure 8, and it is compared with a normal signal intensity variation image. In image 8(a), high intensity means high mobility, and dark areas means slow mobility or presence of gas. For the last one the changes are very big. In the same way, in image 8(b), high intensity means long T_2 values related to high mobility, and low intensity means short T_2values related slow mobility or the presence of gas coming out of solution. Those areas in Figure 8(a) that show the gas channel correlate very well with those in Figure 8(b) having very short or no detectable T_2 values. With this measurement, it is possible to follow the behavior of the most mobile protons from the sample because they will be the ones with longer T_2.

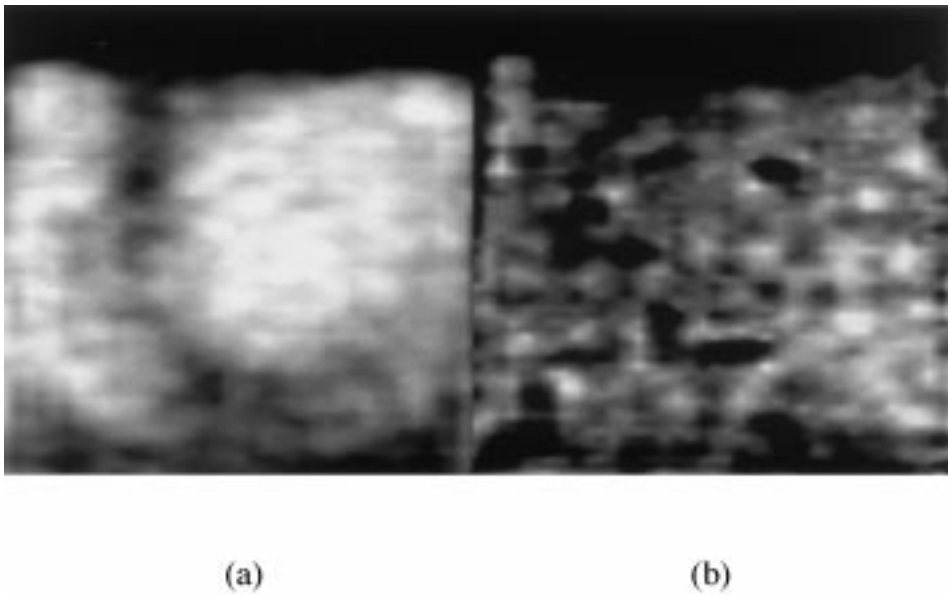

Figure 8. Comparison between signal intensity image (a), and T_2 (b) map for the 1.4 MPa pressure step.

After the maps were calculated, an average value for T_2 was determined at each pressure and with respect to time after the pressure had been changed. These values can be considered as bulk T_2. The plots of pressure versus T_2 for four different times are presented in Figure 9. The data was fitted with a continuous curve to highlight the trend in the values.

At the first time, the T_2 value has an ondulatory behavior with respect to pressure going through a series of maximums, being the highest corresponding to a pressure close to the bubble point for this sample. This high T_2 value is also observed for the same pressure with respect to time. These experimental results are not fully understood at the present time.

An important observation from these data is that the width from the different ondulations gets wider with respect to time. This observation would imply that there is a more homogenous distribution of T_2 values in the sample with respect to time. Homogeneity in T_2 translates to homogeneity in viscosity values, as the sample reaches equilibrium.

As well as T_2, it was also possible to obtain information about the intensity from the first echo in the CPMG pulse sequence, and from T_2 calculation, the value of the spin density (SD) associated to the T_2. Figures 10 and 11, show SD and the first echo signal strength (FESE), respectively. All curves have been fitted in the same way as the T_2 curve.

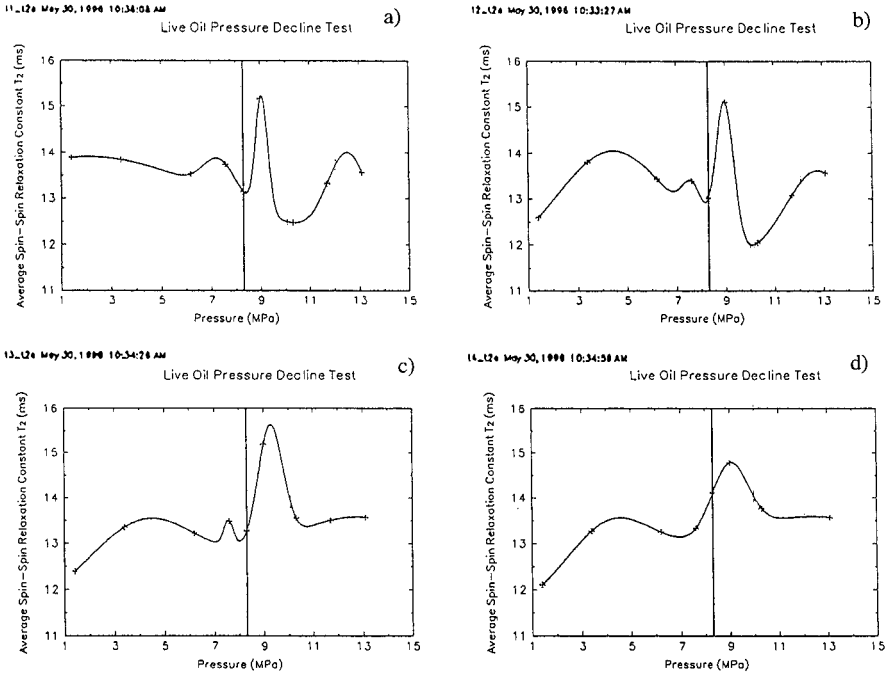

Figure 9. Plots of T_2 versus pressure for four different times after the pressure step. Times after pressure steps are: (a) 5 min, (b) 60 min, (c) 123 min and (d) 180 min.

These plots show a similar ondulatory characteristic as the T_2 curve. One would expect a synchronous patron from the three plots. But a close examination indicates that above the bubble point, the T_2 curve is not in synchronism with SP and FESE, whereas below the bubble point they get in synchronism. We do not have any explanation for that observation and further investigation is needed.

3.3. T_2: VISCOSITY RELATIONSHIP AND OIL VISCOSITY MAPS

A great interest was placed in this work to the possibility of producing a correlation between the spin–spin lattice relaxation times, T_2 , and the viscosity for the live oil. The first step in this direction was to determine independently the relation between viscosity and $T_2$with temperature for each of these variables. The viscosity measurements with respect to temperature for the dead oil and with respect to pressure for the live oil were obtained using a capillary viscometer. The results are presented in Figure 12. For T_2, two types of measurements were carried out, namely CPMG and T_2 maps. The results for the CPMG data are presented in Figure 13.

The next step was to transform the viscosity and T_2 correlation with temperature into one between the two variables of interest. The results are presented in Figure 14 for T_2 CPMG and T_2 map data. The figure shows the fitted curve obtained from the experimental data. T_2 values from the maps are used to produce the viscosity maps

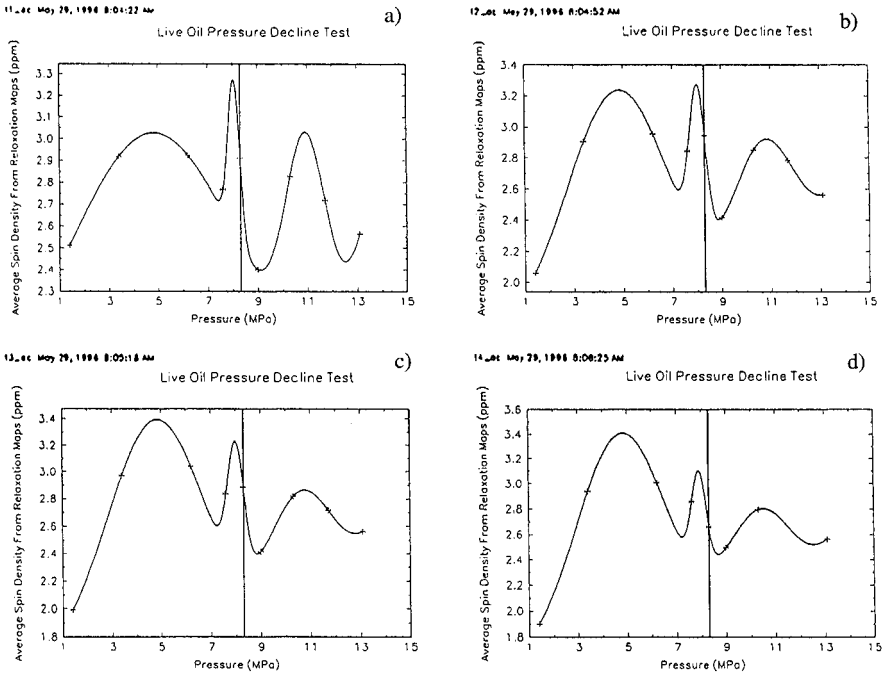

Figure 10. Plots of Spin density versus pressure for four different times after the pressure step: (a) 5 min, (b) 60 min, (c) 123 min and (d) 180 min.

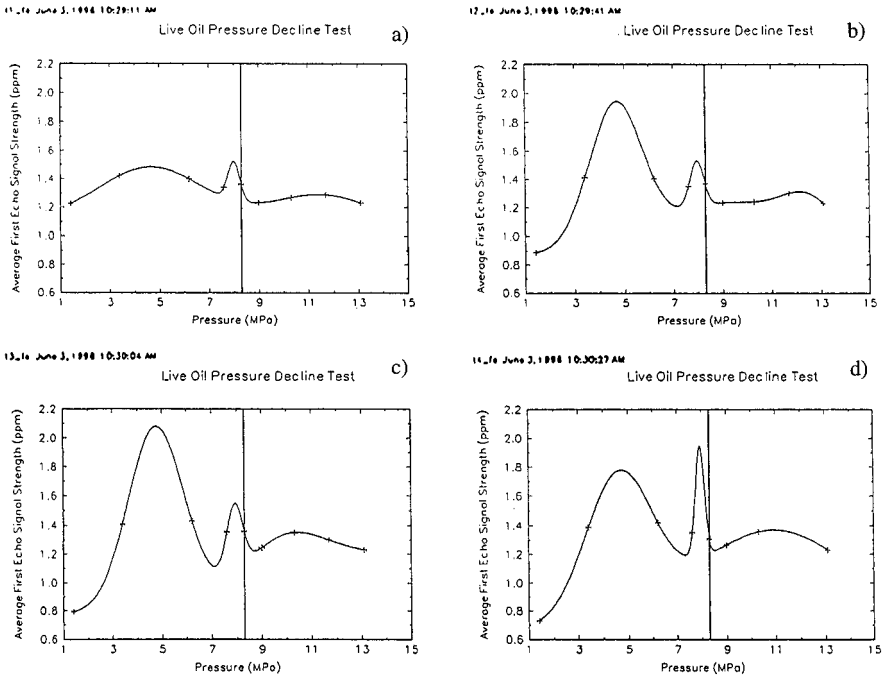

Figure 11. Plots of first echo intensity versus pressure for four different times after the pressure step: (a) 5 min, (b) 60 min, (c) 123 min and (d) 180 min.

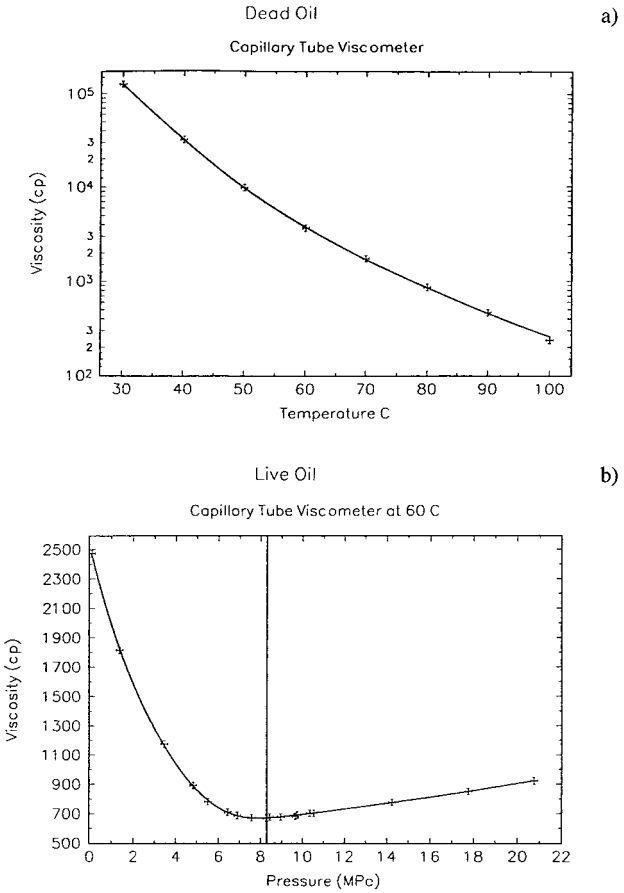

Figure 12. (a) Dead oil viscosity versus temperature using capillary viscometer; (b) Live oil viscosity versus pressure using capillary viscometer at 60°C.

for the live oil as a function of pressure. Viscosity maps were constructed by taking T_2 values from the respective map, and using the correlation obtained from Figure 14 to produce the corresponding viscosity value.

Figure 15 shows the results obtained from this type of transformation for the different pressures, a total of eight. The figure is composed of a pair of viscosity maps for each pressure; the first has been taken immediately after the pressure change, and the second taken at a time t after the pressure change, giving a total of 16 maps. The first two maps at the left hand top of Figure 15 correspond to the pressure change from 13.1 to 11.2 MPa, and the last two maps shown at the right hand bottom correspond to the pressure change from 3.4 to 1.4 MPa.

From Figure 15 we observe that there is not much viscosity change with respect to time for the 11.2 MPa pressure change. However, for the second pressure change, there is a significant, not expected, increase in viscosity across the whole sample for $t = 0$, when compared with the last one from the previous pressure. After a

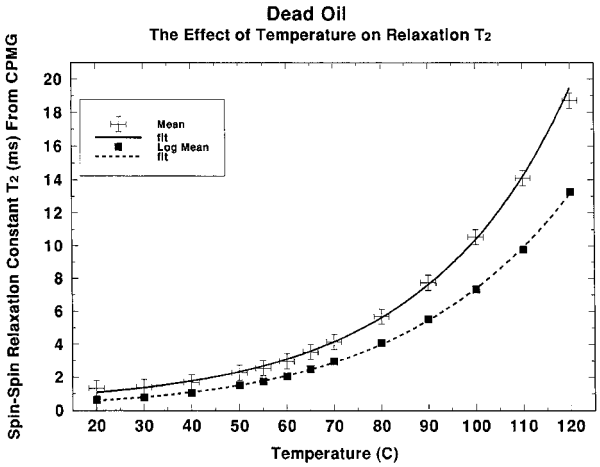

Figure 13. Hamaca dead oil T_2 dependency with temperature obtained from CPMG measurements.

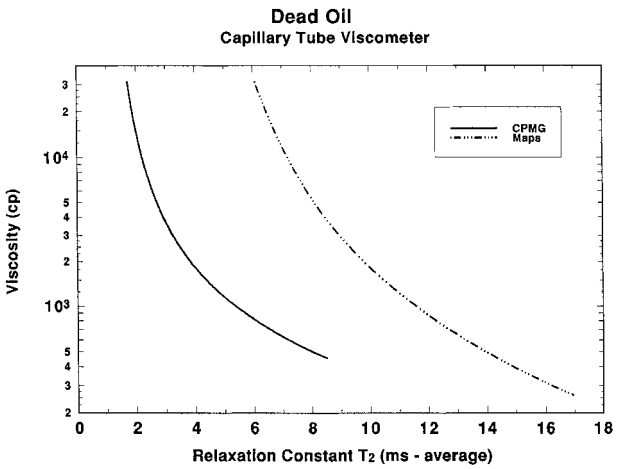

Figure 14. Correlation between viscosity versus T_2 for Hamaca dead oil at 60°C. T_2's from CPMG bulk and T_2 maps.

time *t*, the distribution of viscosity goes back to values similar to those from the first pressure change. Similar patterns were observed for the next two pressure changes (9.0, 8.3 MPa). Those pressure values are above the bubble pressures.

This behavior is reversed below the bubble point. Immediately after the pressure change, the viscosity goes down in comparison to the end of the previous pressure, and after a time *t* the viscosity goes up. The important point is that both above and below the bubble point the viscosity values for the initial times go in the opposite direction than expected, that is, above, it goes to high values before going to low, and below, the viscosity goes to low before going to high values. An analytical method

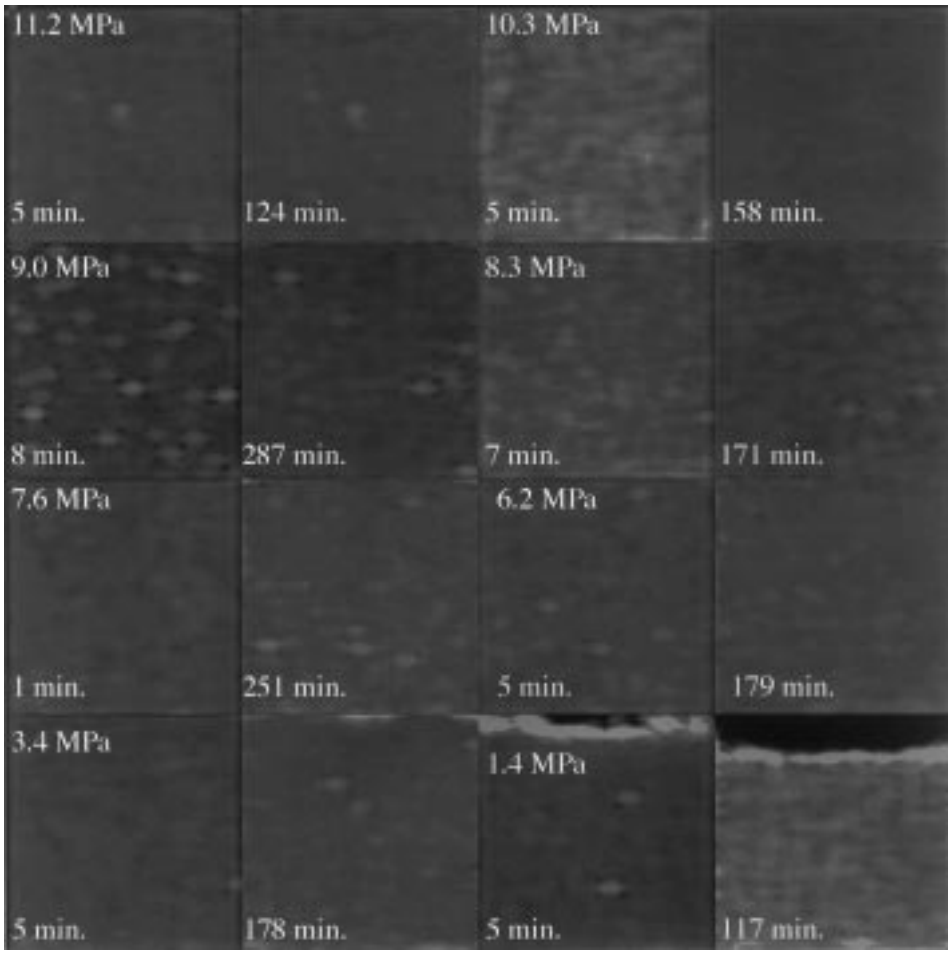

Figure 15. Viscosity maps for Hamaca live oil obtained from the corresponding T_2 maps with respect to pressure.

for the analysis of the viscosity maps has been developed to substitute the present visual evaluation. Further results on this behavior will be presented in a forthcoming publication.

There is another important aspects that was detected at the 1.4 MPa pressure step. The viscosity map for the $t = 0$ shows the presence of the gas cap as it was observed in the intensity image. We also observed a thick layer of sample that has the highest viscosity. For time *t*, the gas cap has increased to a fourth of the whole cell volume, and the layer of high viscosity is still present at the top of the sample. It is important to note that the area of the high viscosity film is only detected when most of the gas has been released from the crude.

The formation of a high viscous layer can be explained as follows: At the beginning of the bubble formation process they could be trapped in a three-dimensional network

formed by oil components of the extra heavy crude oil (Acevedo *et al.*, 1996). As the bubbles grow in size they rise to the top of the core holder taking with them the network. This fraction of the oil has the lowest concentration of dissolved gas, and therefore it has the shortest T_2 that correlates with a very high viscosity. When the bubbles burst, they splash the oil at the top of the liquid phase which can be seen as a high viscosity area.

4. Conclusions

1. The rate at which the bubbles are formed appears to be $\mathrm{d}p/\mathrm{d}t$ dependent.
2. A significant increase in the average T_2 from the maps at the bubble point was observed.
3. A correlation between T_2 and viscosity that allows to produce viscosity maps for the studied sample using MRI was found.
4. Above the bubble point, the viscosity of the sample varies from low to high to low with respect to time after the pressure change. Below the bubble point, the situation is reverse, the viscosity of the sample varies from high to low to high with respect to time after the pressure change. One would expect a monotonic change in viscosity with respect to time.
5. The study shows the potential use of MRI to follow viscosity changes during pressure depletion test in a PVT MRI cell.

References

Fisher, D., Espidel, Y., Huerta, M., Randall, L. and Goldman, J.: 1995, Phase behavior visualization for foamy oils using magnetic resonance imaging, 1996/97-6, Petroleum Recovery Institute–INTEVEP Joint Report, Calgary, Canada.

Morriss, C. E., Freedman, R., Straley, C., Johnston, M., Vinegar, H. J. and Tutunjian, P. B.: 1994, Hydrocarbon saturation and viscosity estimation form NMR logging in the Belridge Diatomite, *SPWLA 35th Annual Logging Symposium*, Paper C, June 19–22, pp. 1–24.

Maini, B., Sheng, J. and Nicola, F.: 1995, Laboratory investigation of foamy oil flow for improved primary production, Draft Final Report SSC N° XSG94-00145-(608), Petroleum Recovery Institute, Calgary, Canada.

Acevedo, S., Escobar, G., Huerta, M., Piña, G. and Hernández, Z.: 1996, Gas trapping mechanism for foamy oil behavior: 3D network of oil components in extra-heavy crude, submitted for publication.